Romanian Reports in Physics **72**, 407 (2020)

OPTICAL FIBER-BASED PLASMONIC SENSORS USING ALUMINIUM OXIDE INSULATOR

V.A. POPESCU

University "Politehnica" of Bucharest, Department of Physics 1,
Splaiul Independentei 313, 060042 Bucharest, Romania
E-mail: *vapopescu@yahoo.com*

Received February 12, 2020

Abstract. The angular and spectral interrogation methods are applied to calculation of the power loss, figure of merit and spectral and amplitude sensitivities for the TM modes in a fiber-based plasmonic sensor with four layers using a very thin aluminium oxide insulator as the interior or exterior cladding layer. The values of the effective indices calculated by using the finite element method are in agreement with an analytical method where the electromagnetic field is represented by a Bessel function of the first kind in the core region (SiO_2), a linear combination of the Hankel functions in the gold and Al_2O_3 regions, and a modified Bessel function of the second kind in the outermost region (H_2O). For a fiber with four layers and the gold layer in the exterior part of the cladding region, the limit of detection in intensity interrogation mode (7.78×10^{-8} RIU) is better than in angular interrogation mode (8.41×10^{-6} RIU).

Key words: sensors, optical fiber, surface plasmon resonance.

1. INTRODUCTION

Optical fiber-based plasmonic sensors are widely used in chemical, biological, and medical monitoring [1–31]. Thus, some plasmonic biosensors [13, 19–20, 29–30] are applied for detection of human-liver tissues, of human blood groups A, B, and O and to measure the hemoglobin concentration in human blood.

The values of the effective indices calculated by using the finite element method are in agreement [10] with an analytical method where a linear combination of the Hankel functions H_1 and H_2 represents the field in the gold region of a fiber-based plasmonic sensor. Also, the difference between the resonant wavelengths calculated with the finite element method and with the analytical method is very small.

The interrogation (angular or spectral) method has been used for the analysis of fiber-based plasmonic sensors [22–26, 28–31].

In this paper, the angular and spectral interrogation methods are applied to an optical fiber-based plasmonic sensor when the dispersions of SiO_2, gold, Al_2O_3 (insoluble in water), and distilled water (H_2O) are considered. The power loss and amplitude sensitivity are increased at optimized thicknesses of the Al_2O_3 and gold layers for the TM mode.

The values of the effective indices calculated by using the finite element method are in agreement with an analytical method where the electromagnetic field is represented by a Bessel function of the first kind in the core region (SiO_2), a linear combination of the Hankel functions in the gold and Al_2O_3 regions due to their complex values of the refractive indices, and a modified Bessel function of the second kind in the outermost region (H_2O).

The paper is structured as follows. In Section 2 we briefly present the structure of the four-layer optical fiber-based plasmonic sensor. The angular and spectral interrogation methods are described in Section 3. We discuss in Section 4 the results of extensive numerical simulations. The summary and the discussion of the obtained results are given in Section 5.

2. OPTICAL FIBER-BASED PLASMONIC SENSOR

Figure 1 shows an optical fiber with four layers (SiO_2, gold, Al_2O_3, and H_2O), where the Al_2O_3 layer can be in the exterior part or in the interior part of the cladding region. The thicknesses of the Al_2O_3 and gold layers are d_a and d_g, respectively.

The refractive index of the SiO_2 [22], Al_2O_3 [32], and distilled water [33] are calculated through a Sellmeier-type relation. The refractive index of the gold layer is calculated by the Drude model [34] as in references [7–10]. For a laser wavelength λ = 1.064 μm, the refractive indices of SiO_2, Al_2O_3, gold, and H_2O are 1.449631, 1.0818 + 9.1074i, 0.378034 + 6.210551i and 1.323917 + 0.0000012193i, respectively.

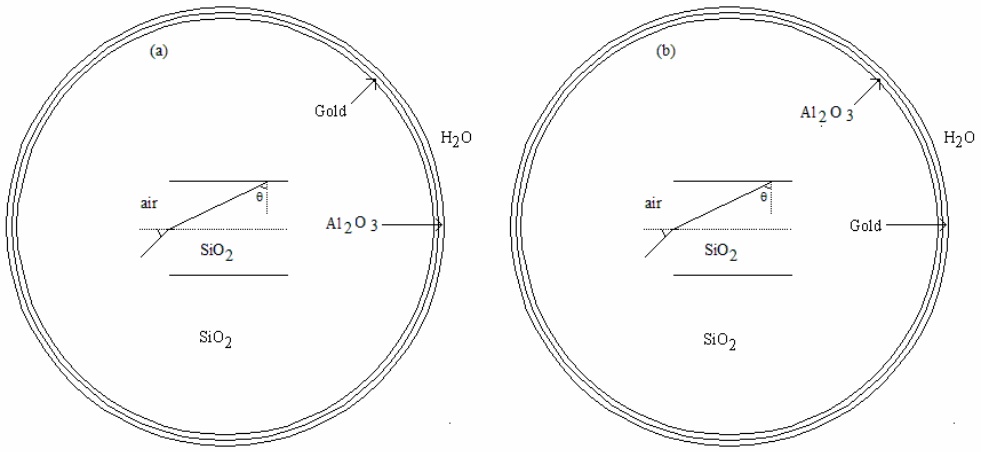

Fig. 1 – Schematic of an optical fiber with four layers (SiO_2, gold, Al_2O_3 and H_2O) in (a) and (SiO_2, Al_2O_3, gold, and H_2O) in (b). The gold layer is in interior in (a) and in exterior in (b). The light is incident from an air medium in a SiO_2 core of the fiber and the angle inside the fiber is θ.

3. ADAPTED ANGULAR AND SPECTRAL INTERROGATION METHODS

In the angular interrogation method [22–26, 28–31], the wavelength is kept constant and the angle of incidence is varied and a sharp dip (maximum of the power loss) appears at a resonance incidence angle θ in the reflectivity. In the spectral interrogation method, the angle of incidence is kept constant and the wavelength is varied. A sharp dip (maximum of the power loss) appears at a wavelength λ in the reflectivity. The resonance incidence angle and the resonance wavelength are dependent on the refractive index of the sensing medium.

The power loss (in dB) for a *TM* mode for a Bragg fiber with $N = 4$ layers is [25–26]:

$$PL = 10\log\frac{1}{P}, \tag{1}$$

where P is the output power:

$$P = R^{\frac{L}{D\tan(\theta)}}, \tag{2}$$

L is the sensing length, D is the fiber core diameter, θ is the angle inside the fiber ($L/D = 25$), R is the corresponding intensity reflection coefficient:

$$R = |r|^2, \tag{3}$$

and r is the amplitude reflection coefficient:

$$r = \frac{(M_{11} + M_{12}q_4)q_1 - (M_{21} + M_{22}q_4)}{(M_{11} + M_{12}q_4)q_1 + (M_{21} + M_{22}q_4)} \tag{4}$$

In the above relation we have

$$M = M_2M_3 = \begin{pmatrix} M_{11} & M_{12} \\ M_{21} & M_{22} \end{pmatrix}, \tag{5}$$

where

$$M_2 = \begin{pmatrix} \cos(\beta_2) & -\dfrac{i\sin(\beta_2)}{q_2} \\ -iq_2\sin(\beta_2) & \cos(\beta_2) \end{pmatrix}, \quad M_3 = \begin{pmatrix} \cos(\beta_3) & -\dfrac{i\sin(\beta_3)}{q_3} \\ -iq_3\sin(\beta_3) & \cos(\beta_3) \end{pmatrix}, \tag{6}$$

$$\beta_2 = \frac{2\pi d_2}{\lambda}\sqrt{n_2^2 - n_1^2 \sin^2(\theta)}, \quad \beta_3 = \frac{2\pi d_3}{\lambda}\sqrt{n_3^2 - n_1^2 \sin^2(\theta)}. \tag{7}$$

The real part of the effective index of the surface plasmonic wave is given by the relation:

$$\mathrm{Re}(\beta / k) = n_1 \sin\theta = \sqrt{\frac{\varepsilon_{gr} n_{ar}^{\ 2}}{\varepsilon_{gr} + n_{ar}^{\ 2}}}, \tag{8}$$

where n_1 is the refractive index of the core layer (SiO_2), θ is the angle inside the fiber, ε_{gr} is the real part of the gold dielectric function, and n_{ar} is the real part of the refractive index of the analyte. For a laser wavelength λ = 1.064 μm, ε_{gr} = –38.428034, n_{ar} = 1.323917, and Re (β /k) = 1.355184.

The sensing performance of the device is determined by the figure of merit (FOM):

$$\mathrm{FOM} = \frac{\delta\theta_{res}}{\Delta n_a \delta\theta_{0.5}} \text{ or } \mathrm{FOM} = \frac{\delta\lambda_{res}}{\Delta n_a \delta\lambda_{0.5}}, \tag{9}$$

and the maximum of the amplitude sensitivity (S_A):

$$S_A = \frac{PL_a - PL}{\Delta n_a} \times \frac{1}{PL}, \ \Delta n_a = 0.001 \text{ RIU}, \tag{10}$$

where $\delta\theta_{res}$ ($\delta\lambda_{res}$) is the shift in resonance angle (wavelength) corresponding to small variation in refraction index of analyte Δn_a, $\delta\theta_{0.5}$ ($\delta\lambda_{0.5}$) is the resonance angular (spectral) width, PL_a is the power loss at $n_a + \Delta n_a$, and PL is power loss corresponding to reference analyte n_a.

For the variation of real part of the refractive index (Δn_a^r = 0.001 RIU), the angular (wavelength) resonance shift is $\Delta\theta_{res}$ ($\Delta\lambda_{res}$) and the resolution is

$$\Delta n_a^L = \frac{\Delta n_a^r}{\Delta\theta_{res}} \Delta\theta_L \text{ or } \Delta n_a^L = \frac{\Delta n_a^r}{\Delta\lambda_{res}} \Delta\lambda_L \tag{11}$$

assuming that the angular (wavelength) detection limit is $\Delta\theta_L = 0.001°$ ($\Delta\lambda_L$ = 0.1 nm). For Δn_a^r = 0.001 RIU, the power loss shift is ΔPL_{res} and the resolution (limit of detection in intensity interrogation mode) is

$$\Delta n_a^L = \frac{\Delta n_a^r}{\Delta PL_{res}} \Delta P_L \tag{12}$$

assuming that the power detection limit (resolution of power measurement) is $\Delta P_L = 0.01$ dB.

4. NUMERICAL RESULTS AND DISCUSSION

Figure 2 shows the power loss *versus* the angle θ (in radians) for the modes TM of a fiber with the gold layer in interior (d_g = 19.7 nm, d_a = 10 nm) part of the cladding region and for a gold layer in exterior (d_g = 25.9 nm, d_a = 10 nm) part of the cladding layer at the laser wavelength λ = 1.064 μm for two values of the refractive index of the analyte (n_a and n_a + 0.001). Figure 3 shows the amplitude sensitivity *versus* the angle θ for the modes TM of a fiber with the gold layer in interior (d_g = 19.7 nm, d_a = 10 nm) part of the cladding region and for a gold layer in exterior (d_g = 25.9 nm, d_a = 10 nm) part of the cladding region at the laser wavelength λ = 1.064 μm.

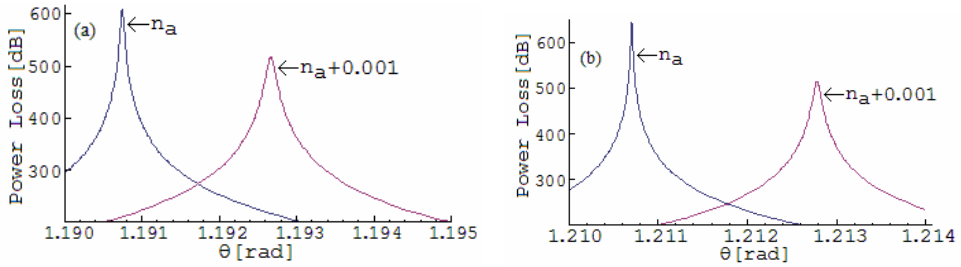

Fig. 2 – Power loss *versus* the angle θ for the modes TM of a fiber with the gold layer in interior (d_g = 19.7 nm, d_a = 10 nm) in (a) and for a gold layer in exterior (d_g = 25.9 nm, d_a = 10 nm) in (b) at the laser wavelength λ = 1.064 μm for two values of the refractive index of the analyte (n_a and n_a + 0.001).

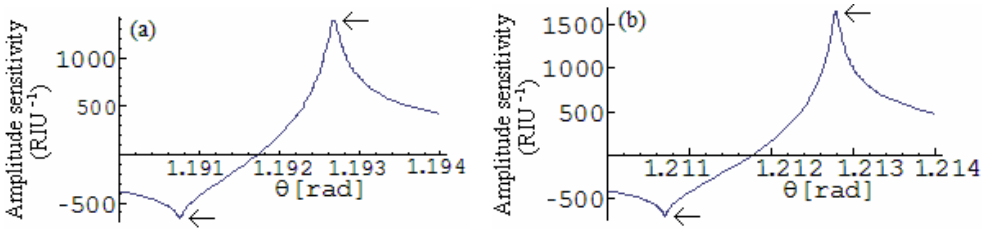

Fig. 3 – Amplitude sensitivity *versus* the angle θ for the modes TM of a fiber with the gold layer in interior (d_g = 19.7 nm, d_a = 10 nm) in (a) and for a gold layer in exterior (d_g = 25.9 nm, d_a = 10 nm) in (b) at the laser wavelength λ = 1.064 μm. The arrows indicate the maximum of the amplitude sensitivity.

For a TM mode, the shift towards higher angles of the maximum power loss PL for an increase Δn_a of the analyte refractive index by 0.001 RIU is $\delta\theta_{res}$ = 0.11° (0.12°), the full width at half maximum (FWHM) of the angular loss is $\delta\theta_{0.5}$ = 0.08° (0.05°), the figure of merit is FOM = 1437.2 RIU^{-1} (2505.6 RIU^{-1}), the maximum of the amplitude sensitivity is S_A=1390.6 RIU^{-1} (1665.5 RIU^{-1}), the maximum value of the power loss is PL = 609.2 dB (642.4 dB), the fixed wavelength is λ = 1.064 μm (1.064 μm), and the difference between maximal amplitude sensitivity and resonant angles is $\Delta\theta_A$ = 0.11° (0.12°) when the gold layer is in the interior (exterior) part of the cladding region.

It is important that real part of the effective index Re (β/k) = n_1 sin θ = 1.449631 sin(68.2249°) = 1.346195 for a fiber (r_1 = 1.3445 μm, d_g = 19.7 nm, d_a = 10 nm) with the gold layer in interior of the cladding region is close to Re (β/k) = 1.346353 calculated for HE_{12} mode by using the analytical method based on the Bessel functions. The effective indices for HE_{11} and HE_{12} modes calculated with this method are β/k = 1.405147 + 0.004102i and β/k = 1.346353 + 0.004103i, respectively. For r_1 = 1.3445 μm, the imaginary parts of the effective indices of the HE_{11} and HE_{12} modes are very close (loss matching point 1 from Fig. 6 and Fig. 7). These values are very close to the calculated values by using the finite element method. On the other hand, the effective indices for TM_{01} and TM_{02} modes calculated with this method for a fiber (r_1 = 1.9296 μm, d_g = 19.7 nm, d_a = 10 nm) with the gold layer in interior of the cladding region are β/k = 1.394065 + 0.0040723i and β/k = 1.348518 + 0.0040721i, respectively. For r_1 = 1.9296 μm, the imaginary parts of the effective indices of the TM_{01} and TM_{02} modes are very close (loss matching point 2 from Fig. 6 and Fig. 7). Also, the real part (1.348518) of β/k for TM_{02} mode is close to the value (1.346195) calculated with the angular interrogation method.

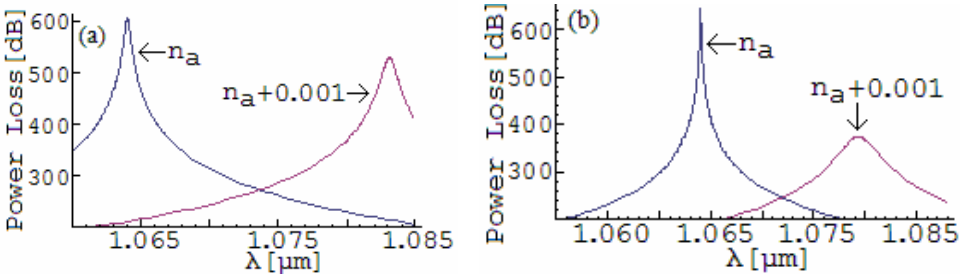

Fig. 4 – Power loss *versus* the wavelength λ for the modes TM of a fiber with the gold layer in interior (d_g = 19.7 nm, d_a = 10 nm) at θ = 68.2249° in (a) and for a gold layer in exterior (d_g = 25.9 nm, d_a = 10 nm) at θ = 69.3684° in (b) near the wavelength λ = 1.064 μm.

Figure 4 shows the power loss *versus* the wavelength λ for the modes TM of a fiber with the gold layer in interior (d_g = 19.7 nm, d_a = 10 nm) at θ = 68.2249° and for a gold layer in exterior (d_g = 25.9 nm, d_a = 10 nm) at θ = 69.3684° near the wavelength λ = 1.064 μm. Figure 5 shows the amplitude sensitivity *versus* the wavelength λ for

the modes TM of a fiber with the gold layer in interior (d_g = 19.7 nm, d_a = 10 nm) at θ = 68.2249° and for a gold layer in exterior (d_g = 25.9 nm, d_a = 10 nm) at θ = 69.3684° near the wavelength λ = 1.064 μm.

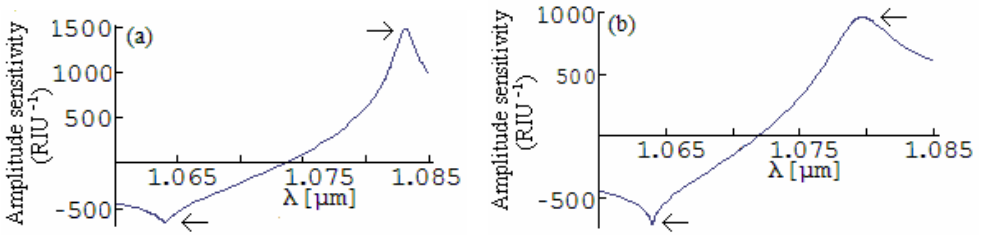

Fig. 5 – Amplitude sensitivity *versus* the wavelength λ for the modes TM of a fiber with the gold layer in interior (d_g = 19.7 nm, d_a = 10 nm) at θ = 68.2249° in (a) and for a gold layer in exterior (d_g = 25.9 nm, d_a = 10 nm) at θ = 69.3684° in (b) near the wavelength λ = 1.064 μm. The arrows indicate the maximum of the amplitude sensitivity.

For a TM mode, the shift towards higher wavelengths of the maximum power loss PL for an increase Δn_a of the analyte refractive index by 0.001 RIU is $\delta\lambda_{res}$ = 19.11 nm (15.34 nm), the full width at half maximum of the loss spectra is $\delta\lambda_{0.5}$ = 13.26 nm (5.91 nm), the figure of merit is FOM = 1440.7 RIU^{-1} (2598.1 RIU^{-1}), the maximum of the amplitude sensitivity is S_A=1481.9 RIU^{-1} (962.8 RIU^{-1}), the maximum value of the power loss is PL = 604.6 dB (646.1 dB), the fixed angle is θ = 68.2249° (69.3684°), and the difference between maximal amplitude sensitivity and resonant wavelengths is $\Delta\lambda_A$ = 19.14 nm (15.66 nm) when the gold layer is in interior (exterior) part of the cladding region.

Figure 6 shows the imaginary part of the effective index of the HE_{11}, HE_{12}, TM_{01} and TM_{02} modes as a function of the core radius r_1 of the fiber with the gold in interior part of the cladding region at a fixed wavelength of 1.064 μm. As the radius of the core layer decreases (increases), the imaginary part of the effective index of the HE_{11}(HE_{12}) and TM_{01}(TM_{02}) modes increases. For r_1 = 1.3445 μm there is a loss matching point between HE_{11} and HE_{12} modes and for r_1 = 1.9296 μm there is a loss matching point between TM_{01} and TM_{02} modes.

Figure 7 shows the imaginary part of the effective index of the HE_{11} and HE_{12} modes at r_1 = 1.3445 μm and for TM_{01} and TM_{02} modes at r_1 = 1.9296 μm as a function of the wavelength λ of the fiber with the gold in interior part of the cladding region near the wavelength of 1.064 μm. As the wavelength decreases (increases), the imaginary part of the effective index of the HE_{12}(HE_{11}) and TM_{02}(TM_{01}) modes increases. For r_1 = 1.3445 μm, there is a loss matching point between HE_{11} and HE_{12} modes and for r_1 = 1.9296 μm there is a loss matching point between TM_{01} and TM_{02} modes. For n_a + 0.001 the loss matching point is at λ = 1.06129 μm for HE_{11} and HE_{12} modes and at λ = 1.05973 μm for TM_{01} and TM_{02} modes.

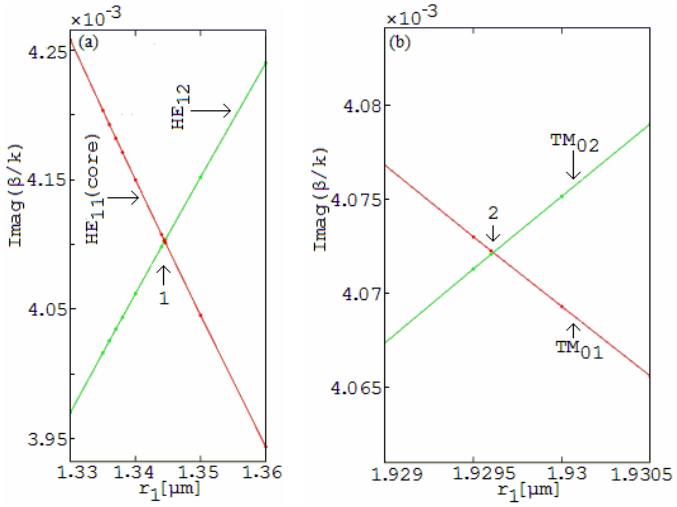

Fig. 6 – The imaginary part of the effective index β/*k versus* the core radius r_1 of a fiber with the gold layer in interior (d_g = 19.7 nm, d_a = 10 nm) for HE_{11} core (red) and HE_{12} (green) modes (a) near r_1 =1.3445 μm (loss matching point 1) and for TM_{01} (red) and TM_{02} (green) modes (b) near r_1 =1.9296 μm (loss matching point 2) (Color online).

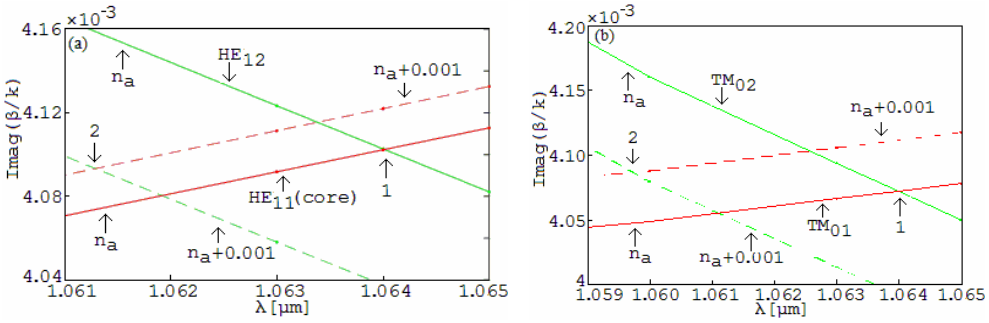

Fig. 7 – The imaginary part of the effective index β/*k versus* the wavelength λ of a fiber with the gold layer in interior (d_g = 19.7 nm, d_a = 10 nm) for HE_{11} core (red) and HE_{12} (green) modes (a) with r_1 =1.3445 μm and for TM_{01} (red) and TM_{02} (green) modes (b) with r_1 =1.9296 μm for two values of the refractive index of the analyte (n_a with the loss matching point 1 and n_a + 0.001 with the loss matching point 2) (Color online).

Table 1 shows the shift $\delta\theta_{res}$ ($\delta\lambda_{res}$) towards higher angles (wavelengths) of the maximum power loss PL for an increase Δn_a of the analyte refractive index by 0.001 RIU, the full width at half maximum (FWHM) of the angular loss $\delta\theta_{0.5}$ (loss spectra $\delta\lambda_{0.5}$), the figure of merit FOM, the maximum of the amplitude sensitivity S_A, the maximum value of the power loss PL, the wavelength λ, the angle inside the fiber θ, and the difference $\Delta\theta_A$ ($\Delta\lambda_A$) between maximal amplitude sensitivity and resonant angles (wavelengths) for a TM mode of a fiber when the gold layer is in the interior part of the cladding region.

Table 1

Values of $\delta\theta_{res}$ [°], $\delta\lambda_{res}$ [nm], $\delta\theta_{0.5}$ [°], $\delta\lambda_{0.5}$ [nm], FOM [RIU^{-1}], S_A [RIU^{-1}], PL [dB], λ [μm], θ [°], $\Delta\theta_A$ [°] and $\Delta\lambda_A$ [nm] for a TM mode of an optical fiber with four layers with the thicknesses d_g [nm] and d_a [nm] of the gold and Al_2O_3 layers, respectively. The gold layer is in the interior of the cladding region

d_g; d_a	$\delta\theta_{res}$ $\delta\lambda_{res}$	$\delta\theta_{0.5}$ $\delta\lambda_{0.5}$	FOM	S_A	PL	λ θ	$\Delta\theta_A$ $\Delta\lambda_A$
19.7; 10	0.11 19.11	0.08 13.26	1437.2 1440.7	1390.6 1481.9	609.2 604.6	1.064 68.2249	0.11 19.14

Table 2

Values of $\delta\theta_{res}$ [°], $\delta\lambda_{res}$ [nm], $\delta\theta_{0.5}$ [°], $\delta\lambda_{0.5}$ [nm], FOM [RIU^{-1}], S_A [RIU^{-1}], PL [dB], λ [μm], θ [°], $\Delta\theta_A$ [°], and $\Delta\lambda_A$ [nm] for a TM mode of an optical fiber with four layers with the thicknesses d_g [nm] and d_a [nm] of the gold and Al_2O_3 layers, respectively. The gold layer is in the exterior of the cladding layer. The last line is for an optical fiber with three layers without Al_2O_3 layer

d_a; d_g	$\delta\theta_{res}$ $\delta\lambda_{res}$	$\delta\theta_{0.5}$ $\delta\lambda_{0.5}$	FOM	S_A	PL	λ θ	$\Delta\theta_A$ $\Delta\lambda_A$
10; 25.9	0.12 15.34	0.05 5.91	2505.6 2598.1	1665.5 962.8	642.4 646.1	1.064 69.3684	0.12 15.66
0; 44.4	0.12 16.42	0.06 8.02	2011.9 2045.8	1747.4 1124.0	577.8 578.6	1.064 69.4685	0.12 16.7

Table 2 shows the same characteristics as in Table 1 for a TM mode of a fiber when the gold layer is in the exterior part of the cladding region. The last line of this Table is for an optical fiber with three layers without Al_2O_3 layer when the optimized thickness of the gold layer is increased at 44.4 nm.

For a TM mode of a plasmonic fiber without an Al_2O_3 layer, the optimized thickness of the gold layer is d_g = 44.4 nm and the sensing characteristics are given in the last line of the Table 2. It is important that the real part of the effective index Re (β/k) = $n_1\sin\theta$ = 1.449631 sin(69.4685°) = 1.357550 for the fiber (r_1 = 1.3468 μm, d_g = 44.4 nm, d_a = 0 nm) is close to Re (β/k) = 1.359846 calculated for HE_{12} mode by using the analytical method based on the Bessel functions. The effective indices for HE_{11} and HE_{12} modes calculated with this method are β/k = 1.405063 + 0.00305421i and β/k = 1.359846 + 0.00305374i, respectively. For r_1 = 1.3468 μm, the imaginary parts of the effective indices of the HE_{11} and HE_{12} modes are very close (loss matching point). These values are very close to the calculated values by using the finite element method. On the other hand, the effective indices for TM_{01} and TM_{02} modes calculated with this method for the fiber (r_1 = 1.9610 μm, d_g = 44.4 nm, d_a = 0 nm) are β/k = 1.396111 + 0.00297159i and β/k = 1.361327 + 0.00297136i, respectively. For r_1 = 1.9610 μm, the imaginary parts of the effective indices of the TM_{01} and TM_{02} modes are very close (loss matching point). Also, the real part (1.361327) of β/k for TM_{02} mode is close to the value (1.357550) calculated with the angular interrogation method.

For an angular detection limit of 0.001°, the sensor angular resolution (8.41×10^{-6} RIU) is smaller for a fiber with four layers when the gold layer is in the exterior part of the cladding region. For the same fiber structure and a power detection limit of 0.01 dB, the sensor power resolution in intensity interrogation mode is 7.78×10^{-8} RIU. Thus, the limit of detection in the intensity interrogation mode is better and more useful than in the angular interrogation mode.

5. CONCLUSIONS

The angular and spectral interrogation methods show that for an optical fiber-based plasmonic sensor with a thin Al_2O_3 insulator layer, the best figure of merit and the maximum of the amplitude sensitivity in the infrared region near the laser wavelength $\lambda = 1.064$ μm are obtained when the gold layer is in the exterior part of the cladding region of the fiber for the distilled water as the analyte layer.

For some values of the core (SiO_2) radius there is a loss matching point between HE_{11} and HE_{12} modes and between TM_{01} and TM_{02} modes when the imaginary parts of the effective indices of the HE_{11} (TM_{01}) and HE_{12} (TM_{02}) modes calculated with an analytical method based on the Bessel functions are very close.

For a fiber with four layers and the gold layer in the exterior part of the cladding region, the limit of detection (7.78×10^{-8} RIU) in the intensity interrogation mode is better than in the angular interrogation mode (8.41×10^{-6} RIU).

It is important to note that the difference $\Delta\theta_A$ ($\Delta\lambda_A$) between maximal amplitude sensitivity and resonant angles (wavelengths) are very close to the shift $\delta\theta_{res}$ ($\delta\lambda_{res}$) towards higher angles (wavelengths) of the maximum power loss PL for an increase Δn_a of the analyte refractive index by 0.001 RIU.

REFERENCES

1. V.A. Popescu, N.N. Puscas, and G. Perrone, J. Opt. Soc. Am. B **29**, 3039 (2012).
2. V.A. Popescu, Mod. Phys. Lett. B **26**, 1250207 (2012).
3. V.A. Popescu, Mod. Phys. Lett. B **27**, 1350038 (2013).
4. V.A. Popescu, N.N. Puscas, and G. Perrone, Eur. Phys. J. D **67**, 215 (2013).
5. V.A. Popescu, N.N. Puscas, and G. Perrone, Eur. Phys. J. D **68**, 229 (2014).
6. V.A. Popescu, N.N. Puscas, and G. Perrone, J. Opt. Soc. Am. B **31**, 1062 (2014).
7. V.A. Popescu, N.N. Puscas, and G. Perrone, J. Opt. Soc. Am. B **32**, 473 (2015).
8. V.A. Popescu and N.N. Puscas, Rom. Rep. Phys. **67**, 500 (2015).
9. V.A. Popescu, N.N. Puscas, and G. Perrone, Plasmonics **11**, 1183 (2016).
10. V.A. Popescu, N.N. Puscas, and G. Perrone, Mod. Phys. Lett. B **30**, 1650075 (2016).
11. V.A. Popescu, Rom. J. Phys. **62**, 204 (2017).
12. V.A. Popescu, N.N. Puscas, and G. Perrone, Plasmonics **12**, 905 (2017).
13. V.A. Popescu, Plasmonics **12**, 1733 (2017).
14. V.A. Popescu, N.N. Puscas, and G. Perrone, J. Opt. **19**, 075004 (2017).
15. V.A. Popescu, N.N. Puscas, and G. Perrone, Optics **6**, 21 (2017).
16. V.A. Popescu, Rom. Rep. Phys. **70**, 404 (2018).

17. V.A. Popescu, J. Phys. Commun. **2**, 015029 (2018).
18. V.A. Popescu, Proc. Romanian Acad. A **19**, 345 (2018).
19. V.A. Popescu, Plasmonics **13**, 575 (2018).
20. V.A. Popescu, Plasmonics **13**, 1507 (2018).
21. V.A. Popescu and A.K. Sharma, OSA Continuum **1**, 496 (2018).
22. A.K. Sharma, R. Jha, and B. D. Gupta, Opt. Commun. **274**, 320 (2007).
23. A.K. Sharma and G.J. Mohr, New J. Phys. **10**, 023039 (2008).
24. B.D. Gupta and R.K. Verma, J. Sens. **979761**, 1 (2009).
25. V.A. Popescu, Rom. J. Phys. **64**, 202 (2019).
26. A.K. Sharma, A. Dominic, B. Kaur, and V.A. Popescu, J. Lightwave Technol. **37**, 5641 (2019).
27. G. Perrone, V.A. Popescu, and N.N. Puscas, Opt. Eng. **58**, 072013 (2019).
28. V.A. Popescu, Rom. Rep. Phys. **71**, 408 (2019).
29. V.A. Popescu and A.K. Sharma, Opt. Quant. Electron. **51**, 290 (2019).
30. V.A. Popescu and A.K. Sharma, Sens. Imaging **21**, 5 (2020).
31. A.K. Sharma, B. Kaur, and V.A. Popescu, Opt. Mater. **102**, 109824 (2020).
32. M.R. Querry, *Optical constants*, Contractor Report CRDC-CR-85034 (1985).
33. S. Kedenburg, M. Vieweg, T. Gissibl, and H. Giessen, Opt. Mater. Express **2**, 1588 (2012).
34. M.A. Ordal, L.L. Long, R.J. Bell, S.E. Bell, R.R. Bell, R.W. Alexander Jr., and C.A. Ward, Appl. Opt. **22**, 1099 (1983).